Green Chemistry

COMMUNICATION

View Article Online
View Journal | View Issue

Cite this: *Green Chem.*, 2025, **27**, 5449

Received 23rd January 2025,
Accepted 25th April 2025

DOI: 10.1039/d5gc00395d

rsc.li/greenchem

Efficient CO_2 electroreduction to *n*-propanol on a matching cobalt phthalocyanine/copper tandem catalyst†

Chunjun Chen,*[a,b] Min Wang,[a,b] Yichi Zhang,[a,b] Xue Yang,[c] Kang Zou,*[c] Wei Lin,*[c] Mingyuan He,[a,b] Haihong Wu[a,b] and Buxing Han*[a,b,d]

Electroreduction of CO_2 into *n*-propanol is a promising strategy to mitigate energy and environmental problems. However, achieving high selectivity of *n*-propanol at high current density remains a challenge. In this work, we report an efficient tandem catalyst by combining cobalt phthalocyanine coordinating with tetrahydrofuran (CoPc-THF) and CuO derived Cu (OD-Cu). The selectivity of *n*-propanol was enhanced over CoPc-THF/OD-Cu tandem catalysts, and the faradaic efficiency (FE) of *n*-propanol reached up to 16.8% with a current density of 170 mA cm^{-2}. It was demonstrated that CO_2 could be converted into CO over CoPc-THF with nearly 100% FE in a wide potential range, which enhances the CO coverage on OD-Cu at a high potential, resulting in high selectivity of *n*-propanol.

Green foundation

1. We report a green and feasible strategy for widening the potential window for CO production over commercial cobalt phthalocyanine (CoPc) by coordinating with tetrahydrofuran (CoPc-THF). Then, an efficient tandem catalyst was prepared by combining CoPc-THF and CuO derived Cu (OD-Cu). *n*-Propanol can be efficiently produced over CoPc-THF/OD-Cu tandem catalysts from the CO_2 electroreduction reaction.
2. The faradaic efficiency (FE) of *n*-propanol reached up to 16.8% with a current density of 170 mA cm^{-2} over CoPc-THF/OD-Cu tandem catalysts. Compared with the state-of-the-art catalysts, the FE of *n*-propanol over CoPc-THF/OD-Cu was the highest with such high current density.
3. In future work, it is desired to develop cheaper catalysts which can produce CO at a wide potential range for constructing feasible tandem catalysts.

Introduction

The electrochemical CO_2 reduction reaction (CO_2RR) has the potential to convert CO_2 and H_2O into a wide range of chemicals and fuels, offering a promising pathway towards achieving carbon neutrality.[1–6] In recent years, various products (such as CO, HCOOH, ethylene, ethanol and *n*-propanol) have been obtained from the CO_2RR.[7–11] Among these products, *n*-propanol is particularly desirable in light of its high energy density and high octane number.[12–15] It is suitable as an engine fuel, as a solvent and as a feedstock for *n*-propyl acetate. However, achieving high selectivity and activity for *n*-propanol is challenging.

The Cu-based catalysts are the most promising electrocatalysts for converting CO_2 into C_{2+} products.[16–19] In recent years, tandem catalysis has been demonstrated as an effective strategy for improving the selectivity of C_{2+} products in the CO_2RR.[20–24] These methods mainly increase the production of the key C1 intermediate (CO) on a Cu-based catalyst by another component to further enhance the production of C_{2+} products, because the selectivity of C_{2+} products can be improved by increasing the coverage of CO. According to previous reports,[25–27] the selectivity of *n*-propanol can be improved by using CO as a reactant, thus we can assume that the design of an efficient tandem catalyst can enhance the selectivity of *n*-propanol from the CO_2RR.

Recently, molecular catalysts/Cu-based tandem catalysts have attracted extensive attention.[28–30] This is because the

[a]*Shanghai Key Laboratory of Green Chemistry and Chemical Processes, State Key Laboratory of Petroleum Molecular & Process Engineering, School of Chemistry and Molecular Engineering, East China Normal University, Shanghai, 200062, China. E-mail: hanbx@iccas.ac.cn*
[b]*Institute of Eco-Chongming, Chongming District, Shanghai, 202162, China*
[c]*State Key Laboratory of Petroleum Molecular and Process engineering, SKLPMPE, Sinopec Research Institute of Petroleum Processing Co., LTD., Beijing 100083, China*
[d]*Beijing National Laboratory for Molecular Sciences, CAS Key Laboratory of Colloid and Interface and Thermodynamics, CAS Research/Education Center for Excellence in Molecular Sciences, Center for Carbon Neutral Chemistry, Institute of Chemistry, Chinese Academy of Sciences, Zhongguancun North First Street 2, Beijing, 100190, P. R. China*

† Electronic supplementary information (ESI) available. See DOI: https://doi.org/10.1039/d5gc00395d

molecular adsorbate generates a high concentration of the key early intermediate, CO, yet does not modulate the metallic active sites germane to the crucial C–C coupling step. For the common commercial molecular catalyst, CO was produced at a low potential, and the potential window was narrow.[31,32] However, the formation of C_{2+} products usually occurred at high potentials over Cu-based catalysts, due to the C–C coupling being related to a high energy barrier.[33,34] Thus, matching the potential window between molecular catalysts and Cu-based catalysts is crucial to build efficient tandem catalysts (Fig. 1a). Widening the potential window for producing CO on a molecular catalyst is an effective strategy to match the potential window of the molecular catalyst and Cu-based catalyst. According to a previous report,[29] a new structure of a molecular catalyst is designed and prepared by introducing functional groups to widen the potential window for producing CO. However, this strategy is time-consuming and costly. Therefore, designing a simple and feasible strategy to widen the potential window for CO production over a commercial molecular catalyst is a much greener approach.

In this work, we report a simple and feasible strategy for matching the potential window between commercial cobalt phthalocyanine (CoPc) and a Cu-based catalyst by widening the potential window for CO production over CoPc. It was found that CO_2 could be converted to CO with nearly 100% selectivity at a wide potential range over CoPc coordinating with tetrahydrofuran (CoPc-THF). Thus, an efficient tandem catalyst was built by combining CoPc-THF and CuO derived Cu (OD-Cu). The selectivity of *n*-propanol was enhanced over CoPc-THF/OD-Cu tandem catalysts, and the faradaic efficiency (FE) of *n*-propanol reached up to 16.8% with a current density of 170 mA cm^{-2}. Experimental and density functional theory (DFT) results revealed that the low-valence CoPc was obtained by coordinating with THF, resulting in high selectivity of CO at wide potentials. Then, the high CO coverage on OD-Cu was achieved, resulting in the high selectivity of *n*-propanol.

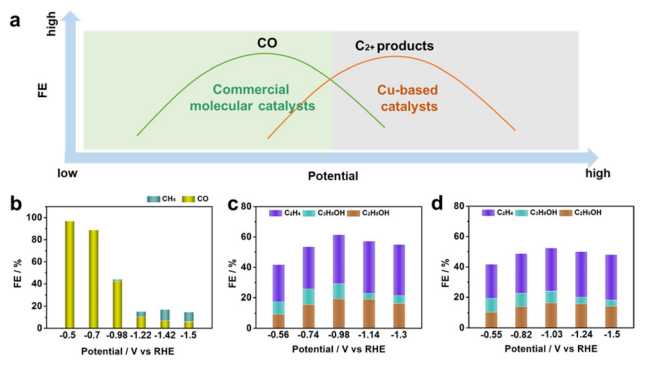

Fig. 1 (a) The diagram of the potential mismatch between the commercial molecular catalyst and Cu-based catalysts. (b) The FE of CO and CH_4 at different potentials over CoPc. (c) The FE of C_{2+} products at different potentials over OD-Cu. (d) The FE of C_{2+} products at different potentials over CoPc/OD-Cu.

Results and discussion

The common commercial CoPc was used as the molecular catalyst for producing the tandem catalyst, because CoPc exhibited a high FE for CO.[31] Firstly, the CO_2RR performance of CoPc was examined in a flow cell with a gas diffusion electrode (GDE) and employing 1 M KOH as the electrolyte. We found that CO_2 can be effectively reduced to CO at low potentials (−0.5 to −0.7 V *vs.* RHE), and the FE of CO was above 90% (Fig. 1b). However, the production of H_2 was significantly enhanced at a high potential (Fig. S1†), and the FE of CO was less than 50% at −0.98 V *vs.* RHE.

In addition, OD-Cu was used as the Cu-based catalyst, because it exhibited a high FE for C_{2+} products. CuO was first prepared (Fig. S2†), and OD-Cu was obtained by *in situ* electroreduction. For OD-Cu, CO_2 can be reduced to C_{2+} products at a high potential (Fig. 1c and Fig. S3†). The maximum FE of total C_{2+} products was 62% at −0.98 V *vs.* RHE; however, the FE of *n*-propanol was only 10.7%.

From the above results, we can find that CO was produced at a low potential over CoPc, and the C_{2+} products were obtained at a high potential over OD-Cu, indicating that the potential window of CoPc and OD-Cu is mismatched. We immobilized CoPc on CuO to prepare the CoPc/CuO catalyst, then CoPc/OD-Cu was obtained by *in situ* electroreduction. For CoPc/OD-Cu, the FE of the C_{2+} products is similar to that of OD-Cu at a low potential (Fig. 1d). However, the FE of C_{2+} products and *n*-propanol over CoPc/OD-Cu was lower than that of OD-Cu at a high potential. This is because the FE of H_2 increased over CoPc at high potentials, resulting in low activity of the CO_2RR (Fig. S4†). Thus, we can assume that matching the potential windows of CoPc and OD-Cu is crucial to enhance the selectivity of *n*-propanol.

Widening the potential window for producing CO on CoPc is an effective strategy to match the potential window of CoPc and OD-Cu. According to a previous report,[35] the CO_2RR performance of CoPc can be tuned by adjusting the electronic structure of Co. To alter the electronic structure of Co in CoPc, THF was used to modify CoPc, because THF exhibited a strong coordination ability. Interestingly, CO_2 can be efficiently reduced to CO at wide potentials over CoPc modified by THF. As shown in Fig. 2a, the FE of CO could reach over 99.0% at −0.46 to −1.3 V *vs.* RHE over CoPc-THF, indicating that the potential window for producing CO of CoPc is widened by coordinating with THF.

Thus, we can assume that CoPc-THF/OD-Cu will be a promising tandem catalyst, because CoPc-THF can provide sufficient CO at a wide potential range, which matches the applied potentials for C_{2+} products over OD-Cu. Then, we immobilized CoPc-THF on CuO to prepare the CoPc-THF/CuO catalyst, and CoPc-THF/OD-Cu was obtained by *in situ* electroreduction. CoPc-THF and OD-Cu were in physically mixed state. The SEM and TEM images (Fig. S5†) confirmed that CoPc-THF/OD-Cu had a nanorod morphology, which is similar to that of CuO. No aggregated CoPc particles can be observed. The energy dispersive X-ray spectroscopy (EDS) study showed a

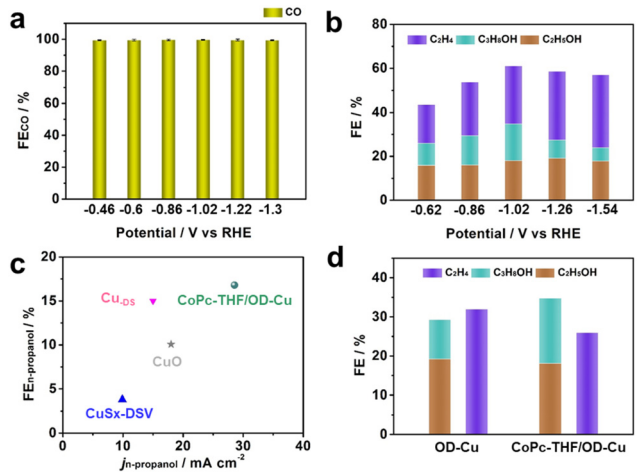

Fig. 2 (a) The FE of CO at different potentials over CoPc-THF. (b) The FE of C_{2+} products at different potentials over CoPc-THF/OD-Cu. (c) Plot of maximum *n*-propanol FE *versus* *n*-propanol partial current density for various catalysts during the CO_2RR. (d) The FE of C_{2+} alcohols (ethanol and *n*-propanol) and ethylene over OD-Cu and CoPc-THF/OD-Cu.

uniform distribution of Co, N, O and Cu elements (Fig. S6†), indicating the CoPc-THF was uniformly dispersed on the OD-Cu catalyst. The X-ray diffraction (XRD) characterization of CoPc-THF/OD-Cu was carried out (Fig. S7†), and the features of CoPc and Cu were observed on CoPc-THF/OD-Cu, suggesting that CoPc-THF/OD-Cu was successfully prepared.

The linear sweep voltammetry (LSV) curves over CoPc-THF/OD-Cu were first determined under CO_2 and N_2 atmospheres (Fig. S8†). The current density over CoPc-THF/OD-Cu in a N_2 environment was obviously lower than that under a CO_2 atmosphere, indicating that the catalyst can promote CO_2 reduction. As shown in Fig. 2b, the total FE of C_{2+} products was enhanced over CoPc-THF/OD-Cu at a low potential. However, the total FE of C_{2+} products over CoPc-THF/OD-Cu was similar to that of OD-Cu at a high potential. In addition, it was noted that the selectivity of *n*-propanol increased over CoPc-THF/OD-Cu, and the maximum FE of *n*-propanol can reach up to 16.8% at −1.02 V *vs.* RHE, which is much higher than that of OD-Cu. Compared with the state-of-the-art catalysts, the FE of *n*-propanol over CoPc-THF/OD-Cu was the highest with such a high current density (Fig. 2c and Table S1†).

The electrochemical data were analyzed and discussed to disclose the enhanced catalytic performance towards *n*-propanol. As shown in Fig. 2d, the FE of the C_{2+} alcohol increased and the FE of C_2H_4 decreased on CoPc-THF/OD-Cu compared to that on OD-Cu. In addition, the overall C_{2+} selectivity only increased slightly on CoPc-THF/OD-Cu, indicating that the selectivity mainly shifts from producing ethylene to alcohols. According to a previous report,[36] the selectivity of products can be changed from C_2H_4 to ethanol by increasing the CO coverage, because the formation of oxygen-containing C_2 intermediates can be enhanced. As shown in Fig. S9,† the FE of CO increased on CoPc-THF/OD-Cu, indicating that CoPc-THF can provide sufficient CO. Thus, we can assume that CoPc-THF can provide sufficient CO to OD-Cu, and then the coverage of CO on OD-Cu can be enhanced, which can increase the formation of oxygen-containing C_2 intermediates. Furthermore, the adsorbed CO can combine with oxygen-containing C_2 intermediates to form C_3 intermediates, leading to high selectivity of *n*-propanol.

The above results indicate that CoPc-THF played an important role in the enhancement of *n*-propanol, which can provide sufficient CO at wide potentials. Then, the intrinsic reason for the efficient CO_2 conversion to CO over CoPc-THF was investigated. It was reported that molecular catalysts can coordinate with small molecules,[37] resulting in distinct properties. Then, the ultraviolet-visible (UV-Vis) absorption spectrum was recorded to explore the coordination between CoPc and THF.[24] When compared to the CoPc solution, these peaks showed a red shift in the CoPc-THF solution, suggesting that CoPc can coordinate with the THF (Fig. S10†).

In addition, to verify the THF coordination with CoPc during the CO_2RR, dimethylsulfoxide was used to dissolve the CoPc molecules on the cathode electrode after the reaction, which was then subjected to spectroscopic characterization. The peaks of THF were observed in the ^{1}H-NMR spectra (Fig. S11†), indicating that THF is stable and coordinates with CoPc during the CO_2RR. In addition, there was no obvious change in both the current density and FE of *n*-propanol during 10 h electrolysis over CoPc-THF/OD-Cu (Fig. S12†), indicating that the catalyst had good stability in the CO_2RR.

To verify the role of THF on the performance of CoPc, the electrochemically active surface areas (ECSAs) of CoPc-THF and CoPc were determined by measuring the double layer capacitance (Fig. S13†). The ECSA of CoPc-THF was similar to that of CoPc, indicating that the excellent activity of CoPc-THF was not due to the change of ECSAs.

It is known that the performance of the CO_2RR depended on the valence state and coordination environment of the catalysts.[10] Thus, the electronic structure of Co in CoPc-THF was explored by X-ray photoelectron spectroscopy (XPS) and X-ray absorption fine spectroscopy (XAFS). As shown in the fine-scanned Co 2p spectra (Fig. 3a), CoPc can be fitted with Co^{2+} (781.5 eV) and Co^{3+} (779.8 eV),[25] and the atomic ratio of Co^{2+} : Co^{3+} is about 1 : 0.07. For CoPc-THF (Fig. 3b), only Co^{2+} was observed, and two obvious satellite peaks located at approximately 786.6 eV and 803.1 eV were observed, which were attributed to the formation of Co^{2+} species.[26] Thus, we can deduce that the electron can transfer from THF (an electron-donating molecule) to CoPc, resulting in a decreasing valence state of Co in CoPc-THF. In the Co K-edge X-ray absorption near-edge structure (XANES), the characteristic absorption peak at 7715 eV (Peak B) was observed for CoPc and CoPc-THF, indicating that the planar Co–N_4 structure of CoPc was not destroyed (Fig. 3c). However, the intensity of peak B of CoPc-THF was weaker than that of CoPc, suggesting that the Co–N_4 structure was distorted. Furthermore, we can find that the curve of CoPc-THF exhibits a minor shift to the left compared with that of CoPc, suggesting that the valence of the Co atom

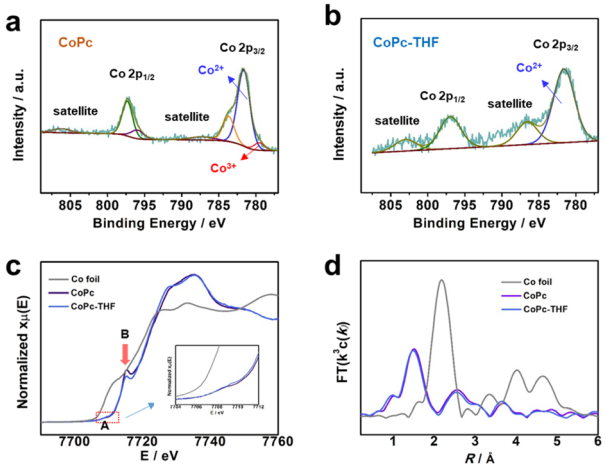

Fig. 3 (a) Deconvoluted Co 3d XPS spectra of CoPc. (b) Deconvoluted Co 3d XPS spectra of CoPc-THF. (c) XANES spectra of different catalysts at the Co K-edge. (d) The corresponding Fourier transforms, FT($k^3w(k)$), of different catalysts.

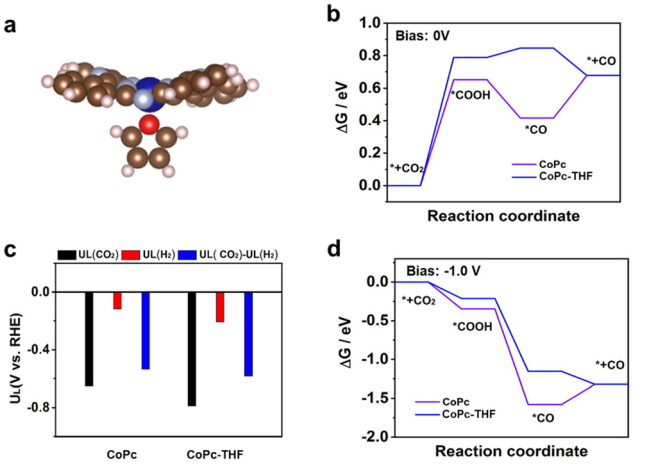

Fig. 4 (a) The model of CoPc/THF. The atoms in blue, cyan, brown, red and pink represent Co, N, C, O and H, respectively. (b) Reaction Gibbs free energy diagrams for the CO_2RR to CO on CoPc and CoPc-THF at 0 V. (c) Difference in limiting potentials for CO_2 reduction and H_2 evolution over CoPc and CoPc-THF. (d) Gibbs free energy diagrams for the CO_2RR to CO on CoPc and CoPc-THF after applying a −1.0 V bias potential.

in CoPc-THF is slightly lower than that of CoPc.[17] These results are consistent with those of the XPS study, indicating a lower valence of Co in CoPc-THF.

From the Fourier transform (FT) extended X-ray absorption fine structure (FTEXAFS), we observed that CoPc exhibits one major peak at about 1.5 Å, which is attributed to the Co–N bond (Fig. 3d). For CoPc-THF, the peaks of Co–N bonds exhibited some deviation compared with those of CoPc, indicating that the coordination environment of the Co atom was changed. In addition, the Co–N and Co–O coordination numbers of CoPc-THF were fitted (Fig. S14, S15 and Table S2†). For CoPc-THF, the Co–N and Co–O coordination numbers were estimated to be 3.8 and 1.0, respectively. Thus, it can be concluded that CoPc coordinated with THF through the Co atom and O atom.

Furthermore, the excellent performance for CO production over CoPc-THF at wide potentials was investigated by DFT simulations. The CoPc molecule with THF was used to represent the model of CoPc-THF (Fig. 4a). As shown in Fig. S16,† the electron density of Co in CoPc-THF is high, suggesting that the electron can transfer from THF to CoPc. Thus, the valence state of Co was lower in CoPc-THF, which is consistent with the results of XPS and XAFS.

As shown in the free energy diagram for the lowest energy pathways of the CO_2RR to CO (Fig. 4b), the activation of CO_2 to form *COOH shows the highest free energy barrier at 0 V. The highest free energy barrier was 0.78 eV for CoPc-THF, which is slightly higher than that over CoPc (0.65 eV). The Gibbs free energy for the dominant competitive hydrogen evolution reaction (HER) was also investigated by DFT calculations (Fig. S17†). The free energy barriers for the formation of H* on CoPc and CoPc-THF are 0.11 eV and 0.21 eV, respectively, indicating that the HER was suppressed over CoPc-THF. Then, the difference between thermodynamic limiting potentials for the CO_2RR and HER ($U_L(CO_2) - U_L(H_2)$) was used to explore the selectivity of the catalysts.[30] The $U_L(CO_2) - U_L(H_2)$ values of CoPc (−0.57 eV) and CoPc/THF (−0.54 eV) are comparable (Fig. 4c), indicating that the selectivity of CO over CoPc-THF and CoPc was similar at low potentials, which is consistent with the performance of the CO_2RR. Furthermore, the reaction energy diagrams were characterized at a negative applied potential (Fig. 4d and Fig. S18†), because CoPc-THF exhibited high selectivity of CO at a high potential. It can be observed that the desorption of CO was endergonic with the highest free energy barrier for CoPc at negative potentials. In contrast, the pathway of the CO_2RR to CO was exergonic over CoPc-THF at a high potential, suggesting that CO_2 can be easily converted to CO. Thus, it can be assumed that the excellent performance of CO generation over CoPc-THF at high potentials was due to the easy desorption of CO.

Conclusions

In summary, an efficient tandem catalyst was built by combining CoPc-THF and OD-Cu. CoPc-THF can provide sufficient CO to OD-Cu, and then high CO coverage on OD-Cu is achieved, resulting in the high selectivity of *n*-propanol. The FE of *n*-propanol reached up to 16.8% with a current density of 170 mA cm^{-2}. Experimental and DFT results revealed that the valence state of Co in CoPc decreased by coordinating with THF, and then the CO desorption on CoPc increased, resulting in high selectivity of CO at wide potentials. Although CoPc is a commercial molecular catalyst, the cost of CoPc is still relatively high. Thus, it is desired to develop a cheaper catalyst which can produce CO at wide potentials for constructing tandem catalysts. We believe that this work can provide guidance in

designing other efficient tandem catalysts for the CO_2RR by matching the potential windows of different catalysts.

Data availability

The data are available within the article and its ESI.†

Conflicts of interest

There are no conflicts to declare.

Acknowledgements

This work was supported by the SINOPEC Research Institute of Petroleum Processing Co., Ltd., National Key Research and Development Program of China (2023YFA1507901) and the National Natural Science Foundation of China (22033009 and 22121002). The X-ray adsorption spectroscopy (XAS) measurements were performed at the 1 W1B beamline at Beijing Synchrotron.

References

1 F. Li, A. Thevenon, A. Rosas-Hernandez, Z. Wang, Y. Li, C. M. Gabardo, A. Ozden, C. T. Dinh, J. Li, Y. Wang, J. P. Edwards, Y. Xu, C. McCallum, L. Tao, Z. Q. Liang, M. Luo, X. Wang, H. Li, C. P. O'Brien, C. S. Tan, D. H. Nam, R. Quintero-Bermudez, T. T. Zhuang, Y. C. Li, Z. Han, R. D. Britt, D. Sinton, T. Agapie, J. C. Peters and E. H. Sargent, *Nature*, 2020, **577**, 509–513.

2 H. Wang, Y. K. Tzeng, Y. Ji, Y. Li, J. Li, X. Zheng, A. Yang, Y. Liu, Y. Gong, L. Cai, Y. Li, X. Zhang, W. Chen, B. Liu, H. Lu, N. A. Melosh, Z. X. Shen, K. Chan, T. Tan, S. Chu and Y. Cui, *Nat. Nanotechnol.*, 2020, **15**, 131–137.

3 J. Gu, C.-S. Hsu, L. Bai, H. M. Chen and X. Hu, *Science*, 2019, **364**, 1091–1094.

4 J. Jiao, R. Lin, S. Liu, W. C. Cheong, C. Zhang, Z. Chen, Y. Pan, J. Tang, K. Wu, S. F. Hung, H. M. Chen, L. Zheng, Q. Lu, X. Yang, B. Xu, H. Xiao, J. Li, D. Wang, Q. Peng, C. Chen and Y. Li, *Nat. Chem.*, 2019, **11**, 222–228.

5 U. O. Nwabara, E. R. Cofell, S. Verma, E. Negro and P. J. A. Kenis, *ChemSusChem*, 2020, **13**, 855–875.

6 D. Yang, Q. Zhu and B. Han, *Innovation*, 2020, **1**, 100016.

7 X. Li, W. Kang, X. Fan, X. Tan, J. Masa, A. W. Robertson, Y. Jung, B. Han, J. Texter, Y. Cheng, B. Dai and Z. Sun, *Innovation*, 2025, **6**, 100807.

8 H. Jung, S. Y. Lee, C. W. Lee, M. K. Cho, D. H. Won, C. Kim, H. S. Oh, B. K. Min and Y. J. Hwang, *J. Am. Chem. Soc.*, 2019, **141**, 4624–4633.

9 W. Ma, S. Xie, T. Liu, Q. Fan, J. Ye, F. Sun, Z. Jiang, Q. Zhang, J. Cheng and Y. Wang, *Nat. Catal.*, 2020, **3**, 478–487.

10 Q. Lei, H. Zhu, K. Song, N. Wei, L. Liu, D. Zhang, J. Yin, X. Dong, K. Yao, N. Wang, X. Li, B. Davaasuren, J. Wang and Y. Han, *J. Am. Chem. Soc.*, 2020, **142**, 4213–4222.

11 X. Dong, X. Sun, S. Jia, S. Han, D. Zhou, T. Yao, M. Wang, M. Fang, H. Wu and B. Han, *Acta Phys.-Chim. Sin.*, 2025, **41**, 100024.

12 J. Li, F. Che, Y. Pang, C. Zou, J. Y. Howe, T. Burdyny, J. P. Edwards, Y. Wang, F. Li, Z. Wang, P. De Luna, C. T. Dinh, T. T. Zhuang, M. I. Saidaminov, S. Cheng, T. Wu, Y. Z. Finfrock, L. Ma, S. H. Hsieh, Y. S. Liu, G. A. Botton, W. F. Pong, X. Du, J. Guo, T. K. Sham, E. H. Sargent and D. Sinton, *Nat. Commun.*, 2018, **9**, 4614.

13 T.-T. Zhuang, Y. Pang, Z.-Q. Liang, Z. Wang, Y. Li, C.-S. Tan, J. Li, C. T. Dinh, P. De Luna, P.-L. Hsieh, T. Burdyny, H.-H. Li, M. Liu, Y. Wang, F. Li, A. Proppe, A. Johnston, D.-H. Nam, Z.-Y. Wu, Y.-R. Zheng, A. H. Ip, H. Tan, L.-J. Chen, S.-H. Yu, S. O. Kelley, D. Sinton and E. H. Sargent, *Nat. Catal.*, 2018, **1**, 946–951.

14 M. Luo, Z. Wang, Y. C. Li, J. Li, F. Li, Y. Lum, D. H. Nam, B. Chen, J. Wicks, A. Xu, T. Zhuang, W. R. Leow, X. Wang, C. T. Dinh, Y. Wang, Y. Wang, D. Sinton and E. H. Sargent, *Nat. Commun.*, 2019, **10**, 5814.

15 P.-P. Yang, X.-L. Zhang, F.-Y. Gao, Y.-R. Zheng, Z.-Z. Niu, X. Yu, R. Liu, Z.-Z. Wu, S. Qin, L.-P. Chi, Y. Duan, T. Ma, X.-S. Zheng, J.-F. Zhu, H.-J. Wang, M.-R. Gao and S.-H. Yu, *J. Am. Chem. Soc.*, 2020, **142**, 6400–6408.

16 P. Grosse, D. Gao, F. Scholten, I. Sinev, H. Mistry and B. R. Cuenya, *Angew. Chem., Int. Ed.*, 2018, **57**, 6192–6197.

17 C. Chen, X. Sun, X. Yan, Y. Wu, M. Liu, S. Liu, Z. Zhao and B. Han, *Green Chem.*, 2020, **22**, 1572–1576.

18 C. Choi, T. Cheng, M. F. Espinosa, H. Fei, X. Duan, W. A. Goddard 3rd and Y. Huang, *Adv. Mater.*, 2018, e1805405.

19 Y. Li, D. Kim, S. Louisia, C. Xie, Q. Kong, S. Yu, T. Lin, S. Aloni, S. C. Fakra and P. Yang, *Proc. Natl. Acad. Sci. U. S. A.*, 2020, **117**, 9194–9201.

20 J. Kim, W. Choi, J. W. Park, C. Kim, M. Kim and H. Song, *J. Am. Chem. Soc.*, 2019, **141**, 6986–6994.

21 D. Gao, I. Sinev, F. Scholten, R. M. Aran-Ais, N. J. Divins, K. Kvashnina, J. Timoshenko and B. R. Cuenya, *Angew. Chem., Int. Ed.*, 2019, **58**, 17047–17053.

22 J. J. Lv, M. Jouny, W. Luc, W. Zhu, J. J. Zhu and F. Jiao, *Adv. Mater.*, 2018, **30**, e1803111.

23 T. C. Chou, C. C. Chang, H. L. Yu, W. Y. Yu, C. L. Dong, J. J. Velasco-Velez, C. H. Chuang, L. C. Chen, J. F. Lee, J. M. Chen and H. L. Wu, *J. Am. Chem. Soc.*, 2020, **142**, 2857–2867.

24 Q. Zhu, X. Sun, D. Yang, J. Ma, X. Kang, L. Zheng, J. Zhang, Z. Wu and B. Han, *Nat. Commun.*, 2019, **10**, 3851.

25 J. Huang, C. N. Borca, T. Huthwelker, N. S. Yüzbasi, D. Baster, M. E. Kazzi, C. W. Schneider, T. J. Schmidt and E. Fabbri, *Nat. Commun.*, 2024, **15**, 3067.

26 Y. Zhou, F. Che, M. Liu, C. Zou, Z. Liang, P. De Luna, H. Yuan, J. Li, Z. Wang, H. Xie, H. Li, P. Chen, E. Bladt, R. Quintero-Bermudez, T. K. Sham, S. Bals, J. Hofkens,

D. Sinton, G. Chen and E. H. Sargent, *Nat. Chem.*, 2018, **10**, 974–980.

27 F. Li, Y. C. Li, Z. Wang, J. Li, D.-H. Nam, Y. Lum, M. Luo, X. Wang, A. Ozden, S.-F. Hung, B. Chen, Y. Wang, J. Wicks, Y. Xu, Y. Li, C. M. Gabardo, C.-T. Dinh, Y. Wang, T.-T. Zhuang, D. Sinton and E. H. Sargent, *Nat. Catal.*, 2020, **3**, 75–82.

28 X. Wang, J. F. de Araujo, W. Ju, A. Bagger, H. Schmies, S. Kuhl, J. Rossmeisl and P. Strasser, *Nat. Nanotechnol.*, 2019, **14**, 1063–1070.

29 R. Kas, R. Kortlever, A. Milbrat, M. T. M. Koper, G. Mul and J. Baltrusaitis, *J. Phy. Chem. Lett.*, 2014, **16**, 12194–12201.

30 J. Wu, S. Ma, J. Sun, J. I. Gold, C. Tiwary, B. Kim, L. Zhu, N. Chopra, I. N. Odeh, R. Vajtai, A. Z. Yu, R. Luo, J. Lou, G. Ding, P. J. A. Kenis and P. M. Ajayan, *Nat. Commun.*, 2016, **7**, 13869.

31 Y. Song, W. Chen, C. Zhao, S. Li, W. Wei and Y. Sun, *Angew. Chem., Int. Ed.*, 2017, **56**, 10840–10844.

32 Y. Jiao, Y. Zheng, P. Chen, M. Jaroniec and S. Z. Qiao, *J. Am. Chem. Soc.*, 2017, **139**, 18093–18100.

33 Y. Song, R. Peng, D. K. Hensley, P. V. Bonnesen, L. Liang, Z. Wu, H. M. Meyer, M. Chi, C. Ma, B. G. Sumpter and A. J. Rondinone, *ChemistrySelect*, 2016, **1**, 6055–6061.

34 T. Sharifi, G. Hu, X. Jia and T. Wågberg, *ACS Nano*, 2012, **6**, 8904–8912.

35 H. Yang, Y. Wu, Q. Lin, L. Fan, X. Chai, Q. Zhang, J. Liu, C. He and Z. Lin, *Angew. Chem., Int. Ed.*, 2018, **57**, 15476–15480.

36 F. Li, Y. C. Li, Z. Wang, J. Li, D.-H. Nam, Y. Lum, M. Luo, X. Wang, A. Ozden, S.-F. Hung, B. Chen, Y. Wang, J. Wicks, Y. Xu, Y. Li, C. M. Gabardo, C.-T. Dinh, Y. Wang, T.-T. Zhuang, D. Sinton and E. H. Sargent, *Nat. Catal.*, 2020, **3**, 75–82.

37 F. A. Walker, D. Beroiz and K. M. Kadish, *J. Am. Chem. Soc.*, 1976, **98**, 3484–3489.